THE JOURNAL OF PHYSICAL CHEMISTRY C

Article

pubs.acs.org/JPCC

Optical Printing of Electrodynamically Coupled Metallic Nanoparticle Arrays

Ying Bao, Zijie Yan, and Norbert F. Scherer*

The James Franck Institute and Department of Chemistry, The University of Chicago, 929 East 57th Street, Chicago, Illinois 60637, United States

Supporting Information

ABSTRACT: Optical forces acting on metallic nanoparticles can be used to organize mesoscale arrays for various applications. Here, we show that silver nanoparticles can be deposited as ordered arrays and chains on chemically modified substrates using a simple and facile optical trapping approach that we term "optical printing". The deposited patterns show preferred separations between nanoparticles resulting from their electrodynamic coupling (i.e., optical binding) in the electromagnetic field of the optical trapping beam. Centrosymmetric optical traps readily allow simultaneous deposition of nanoparticle pairs and triples maintaining the interparticle geometries present in solution. Repositioning an optical line trap with small intercolumn separations allows selectively sampling low and high energy parts of the interparticle potentials. We find that the preferred particle arrangements controllably change from rectangular and triangular to near-field aggregates as one forces the separation to be small. The separation affects the interactions. Interpretation of the results is facilitated by electrodynamic simulations of optical forces. This optical printing approach, which enables efficient fabrication of dense nanoparticle arrays with nanoscale positional precision, is being employed for quantum optics and enhanced sensing measurements.

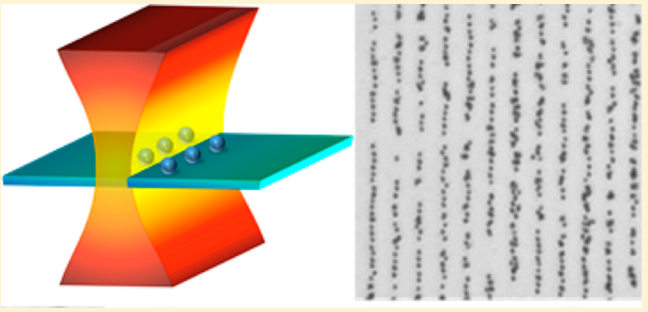

INTRODUCTION

Immobilization of nanoparticles onto solid substrates with desired configurations and patterns is essential in fabricating structures for enhanced sensing and even driving chemical reactivity.[1−7] Minimizing damage to the nanoparticles during the fabrication process and maximizing the accuracy and precision of their deposited positions are important in determining the functionality and performance of the final devices. Fabrication methods such as e-beam lithography, dewetting, inkjet printing, and self-assembly are extensively used to make nanopatterns for a variety of applications, including ultrasensitive detectors, optoelectronic devices, and Nano-Electromechanical Systems.[8−10] For example, Radha et al. reported a fabrication of Au nanoparticle arrays achieved with direct-write e-beam lithography with sub-100 nm spacing.[11] However, top-down approaches typically create materials with defects and concomitantly diminished photonic performance (e.g., greater plasmon damping). On the other hand, self-assembly of colloidally synthesized nanoparticles (a bottom-up approach) typically results in those structures that are thermodynamically most stable. Open challenges remain, particularly to position particles precisely and to form them into more general (i.e., not the thermal favored) arrays.

Optical trapping allows facile manipulation of various nanoscale objects in solution in a contactless manner.[12−19] Optical trapping with a tightly focused laser beam has been used as a "laser printing" method to deposit nanoparticles on solid substrates.[20−22] Because thermal forces that cause particles to fluctuate in position are ubiquitous in solution and in order to minimize the complexity of interparticle interactions, most reports so far are limited to only modest precision and relatively large interparticle separation, typically >1 μm for the latter.[21−23] However, in a few cases, the precision of positioning was better than 100 nm, but this is achieved by sequential deposition of single particles.[22,24]

New strategies for nanoparticle deposition, including preparing large arrays with small interparticle separations, could have an important role in creating new photonic devices. The strong electrodynamic interactions of metal nanoparticles in minimally shaped optical beams make possible a new approach for creating ordered particle arrays combining self-organization and guided assembly.[12,25,26] These interactions, known as optical binding,[27,28] allow creating arrays of metallic nanoparticles with precise interparticle spacing, even such that multiparticle arrays behave as rigid bodies in solution.[12,25,29] The challenge and opportunity is to harness these mesoscale electrodynamic interactions to create nanoparticle patterns with controlled nanoscale precision on substrates.

Received: June 28, 2014
Revised: July 27, 2014

   dx.doi.org/10.1021/jp506443t | J. Phys. Chem. C XXXX, XXX, XXX−XXX

Here, we report the controlled deposition of optically trapped and electrodynamically interacting plasmonic silver nanoparticle arrays (chains and patterns) onto chemically modified solid substrates, an approach that we term "optical printing". We show that local environmental factors, such as the charge density of chemically modified substrates, and the electrodynamic interactions of Ag nanoparticles in a shaped optical trap[26] with pre-existing nanoparticles on the substrate, can significantly influence the deposition of subsequent silver nanoparticles. The particle spacing and geometries were analyzed and compared with the predictions of optical binding theory and finite-differential time-domain (FDTD) numerical simulations. Together, our results demonstrate that optical printing is a facile method to fabricate nanoparticle arrays with control of mesoscale structure and nanoscale precision.

METHODS

Materials. The Ag nanoparticles (reported mean diameter: 200 nm ± 10 nm) were purchased from nanoComposix, Inc. Polyethylenimine (50 wt % in water, branched, average $M_w \sim$ 750k) was purchased from Aldrich. The polyvinylpyrrolidone (PVP)-coated Ag nanoparticles are negatively charged and well-dispersed in water.

Surface Modification. Two walls of the sample cell, including the surface for deposition, were standard no. 1.5 glass coverslips (Fisher Scientific). We treated the coverslips that would become the top surface of the sample cell with piranha solution [3:1 (v/v) H_2SO_4/H_2O_2] for 30 min. These substrates were rinsed with Nanopure water at least three times and then dried with N_2 gas. For the preparation of PEI-modified surfaces, the cleaned coverslips were immersed in a poly(ethylenimine) (PEI) solution at a specific pH for 30 min and again dried with N_2. The substrates were rinsed gently with Nanopure water and dried with N_2 flow for further experiments.

Optical Trapping Instrument, Electrodynamic Simulations, and Optical Printing. The setup for optical trapping experiments was the same as that previously described.[25,28] The constructed light field (i.e., a ring trap, Gaussian trap, or line trap) in this work was generated by a programmable spatial light modulator (SLM, Hamamatsu Photonics X10468 Series). The laser power was measured to be approximately 60 mW before the objective, (60×, water immersion, Olympus UPLSAPO, NA = 1.2). The Ag nanoparticles were visualized by bright-field microscopy. Two beam expanders (1.6× and 2×) internal to the inverted microscope (Olympus IX71) were used to further magnify the optical images on array detectors (Andor Neo sCMOS and Sony XCD-V60CR CCD) that were used to monitor the deposition process and to acquire optical images. The optical forces were calculated using Lumerical "FDTD solution" software, and details of the calculation were described previously.[26]

RESULTS

Details of the optical trapping setup were described previously.[25,29] Briefly, the optical beams, which were focused at the coverslip surface and used to confine Ag nanoparticles in the light field, were generated by a SLM as shown in Figure 1a. In the present study, three kinds of optical traps, as shown in Figure 1b–d, were used for optical printing, including a ring-shaped trap, a Gaussian trap, and line traps. In our previous work, we showed that nanoparticles tend to follow the switching from one trap shape to another.[26] In the earlier

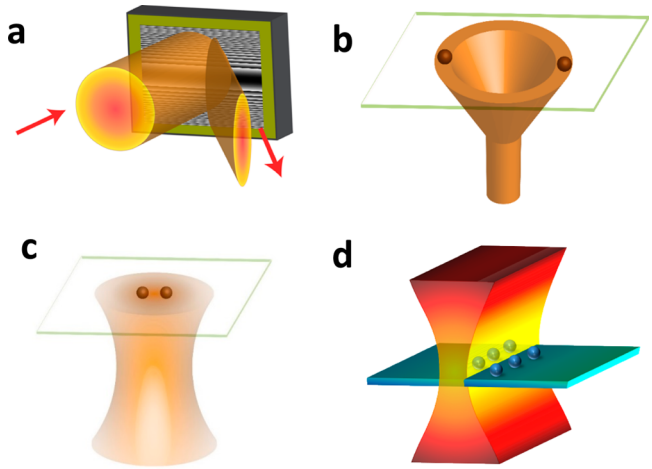

Figure 1. Schematic for optical printing. (a) A SLM and various phase masks were used to generate different optical beam shapes at a transparent substrate as depicted in (b)–(d): (b) Ring-shaped trap with low power density; (c) Gaussian trap with high power density; (d) line trap with intermediate power density. Both the shape of the trap potential and the power density influence the particle array geometry in solution and on surfaces.

work, we used this property to repeatedly sample the paths for formation of nanoparticle clusters in the trap and compare these findings to the potential energy surface that governs the self-organization of metal nanoparticle clusters.[26] In the present experiments, the desired number of silver nanoparticles was first collected in the ring trap and then they were confined into the focused Gaussian trap so that they could be pushed onto the chemically modified substrate for deposition. We tuned the electrostatic charge density of the solid substrate's surface and hence the interaction with nanoparticles so that the resulting cluster was optically printed on the surface will favor the formation of certain structures that were formed in the optical trap.[26] Although optical printing can result in Ag nanoparticles in particular patterns, as shown below, understanding the interactions between the laser beam and nanoparticles during the optical printing process is crucial for controlling the patterning.

Tuning Surface Charge. As just mentioned, the chemical and electrostatic properties of the surfaces (i.e., the solid substrate and also of the nanoparticles) play a critical role in the formation of nanoparticle arrays by optical printing. For controlled deposition and optical printing, one wants sufficiently large electrostatic repulsion to prevent spontaneous deposition of Ag nanoparticles. However, if the repulsive potential is too strong, it would impede deposition with the optical trap. Tuning the surface charge allows facile adjustment and optimization of the DLVO potential.[22,30,31]

We studied the effect of charge density of the substrate on the interaction between the nanoparticles and substrate. Commercial spherical PVP-coated Ag nanoparticles (200 nm in diameter) in aqueous solution (pH 6.44) were used for all experiments. PEI solutions at various pHs were used to modify the glass substrates. The amine groups of the PEI polymer become protonated under acidic conditions; the pK_a values of branched PEI are 4.5 for primary, 6.7 for secondary, and 11.6 for tertiary amine groups.[32] Most amine groups will be protonated at pH < 3, and therefore, the density of positive charges of the PEI-coated glass substrate will also be tuned by the acidity conditions.[33] The glass substrates were cleaned by

dx.doi.org/10.1021/jp506443t | J. Phys. Chem. C XXXX, XXX, XXX–XXX

piranha solution, which creates a negatively charged surface. These cleaned glass substrates were then immersed in the aforementioned PEI solutions and dip-coated.[34] Consequently, the substrate modified with various PEI coatings can have different affinities for the PVP-coated silver nanoparticles.

Optical Printing with Different Surface Charges and Laser Patterns. As shown in Figure 2, three substrates, modified with PEI solutions of different pHs, were used to deposit Ag nanoparticles by optical trapping with a ring pattern laser trap (Figure 1b). A substrate treated with basic PEI solution (pH 10.4) did not allow any nanoparticles to adhere. The substrate treated with acidic PEI solution (pH 2.1) allowed creating a nicely controlled ring pattern of nanoparticles. However, the substrate treated with strongly acidic PEI solution (pH 1.4) showed spontaneous deposition of silver nanoparticles at random locations. These results demonstrate that deposition of Ag nanoparticles depends on the surface charge and DLVO potential energy barrier between the nanoparticle and surface.[31] In particular, since the piranha-cleaned substrates are negatively charged and PEI can be protonated, the sign of the surface change can be tuned from negative to positive. Further discussion on the repulsive forces of the modified substrates decrease with the increase of the acidity of the PEI solution is presented in the Supporting Information.

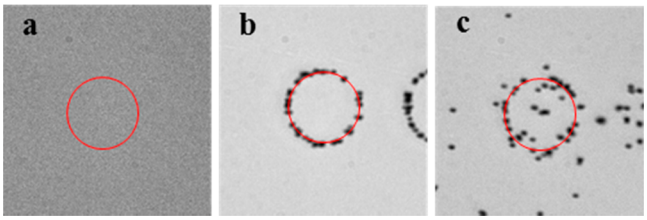

Figure 2. Optical images of Ag nanoparticles deposited on substrates with various surface charges. Red circle (~6 μm in diameter) indicates the location of the ring trap. Substrates were treated with PEI solutions at different pH values: (a) pH = 10.4; (b) pH = 2.2; (c) pH = 1.2. The effect of surface charge was corroborated by quantifying the densities of Ag nanoparticles adsorbed on the substrates modified with PEI solutions of different pH values (Figure S1, Supporting Information). Optical printing cannot cause particle deposition in (a), while the surface charge density in (c) allows even spontaneous particle deposition.

Ordered and oriented Ag nanoparticle clusters were optically printed on a PEI-modified substrate as shown in Figure 3a. Ag nanoparticles were deposited on the substrates with controlled laser power density, and several particles could be deposited simultaneously, i.e., codeposited. During codeposition, a controlled number of Ag nanoparticles were first captured by a ring trap (low power density) without their being adhered to the glass substrate. After switching to a Gaussian trap (high power density), those Ag nanoparticles were confined in the center of Gaussian trap and then rapidly deposited on the PEI-modified substrate. The success rate of dimer printing was more than 80% for large 10 μm scale arrays (i.e., the other 20% were singles or trimmers). The two-step optical trapping and codeposition allows rapidly fabricating nanoparticle dimer arrays with a well-controlled orientation and uniform separation. Figure 3b is an array of silver nanoparticle dimers formed by individual sequential deposition shown for comparison. It is clear that most of clusters in Figure 3b either are aggregated silver nanoparticles and/or have more than two nanoparticles. These aggregated formations are created by

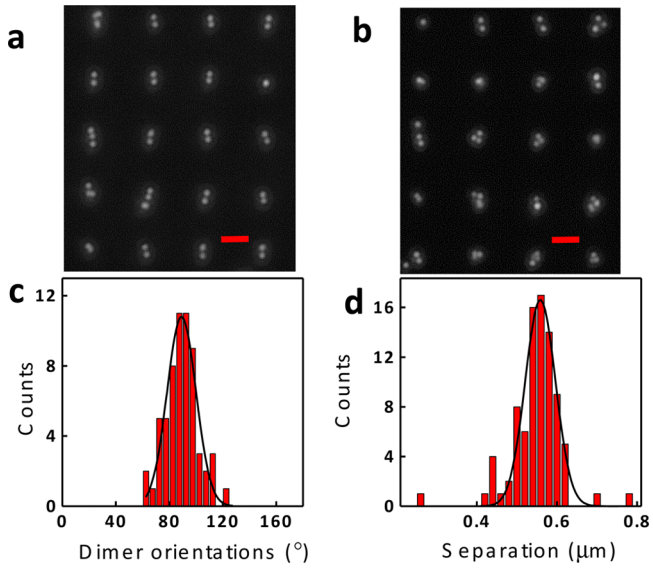

Figure 3. Dark-field images of optically printed Ag nanoparticle arrays and their properties. (a) An array of nanoparticle dimers was printed by simultaneously codepositing pairs of particles. (b) A nanoparticle array was printed wherein each particle deposited sequentially. The red scale bar is 2 μm. (c) The orientational distribution of Ag nanoparticle dimers printed by codeposition in (a). From the best fit Gaussian distribution (black curve), we determine the center and standard deviation of the distribution to be 89° ± 10° to the polarization direction of the trapping laser. (d) The distribution of interparticle separations for Ag nanoparticle dimers created by codeposition. The black curve is a Gaussian fit to the distribution with a center and standard deviation of 559 nm ± 36 nm. The sequentially deposited particle arrays are more disordered, and we omit showing the analogous distributions as (c and d).

using an intense Gaussian beam only. Figure 3c shows the distribution of orientations for the codeposited dimers in relation to the polarization direction of the trapping laser (horizontal direction in Figure 3a). The data for more than 50 deposited dimers clearly show that the dimers are oriented perpendicular to the laser polarization (89°) with a small standard deviation (10°). The (center-to-center) separation of Ag nanoparticles in the dimer array (Figure 3d) shows a narrow Gaussian distribution centered at 559 nm with a standard deviation of 36 nm. This separation is consistent with our expectations based on past studies of optical binding on Ag nanoparticles in solution.[25]

Formation of Extended Ordered Arrays. Since there is a stochastic aspect to the codeposition just described, making extended arrays requires an aspect of deterministic control. In an upgraded version of optical printing, rapid image analysis and computer control could automate this step. We used an anisotropic optical field, a line trap, in combination with precision mechanical movement of a closed-loop 2D-piezo stage for deposition of extended Ag nanoparticle chains in well-defined arrays. The line trap can draw multiple Ag nanoparticles from solution and confine them into chainlike configurations. The x-axis is the direction of laser polarization and the optical line trap is extended along the y-axis direction. Since the laser intensity was made nonuniform along the line trap (y-axis in the images), the trapped nanoparticle located at the highest intensity portion of the line trap tended to deposit first on the PEI-modified substrate. After one or a few particles deposited, the piezo stage was moved by 1 μm increments

dx.doi.org/10.1021/jp506443t | J. Phys. Chem. C XXXX, XXX, XXX−XXX

along the positive y-axis direction in Figure 4a. As a result, linear chains of well-spaced Ag nanoparticles were fabricated on

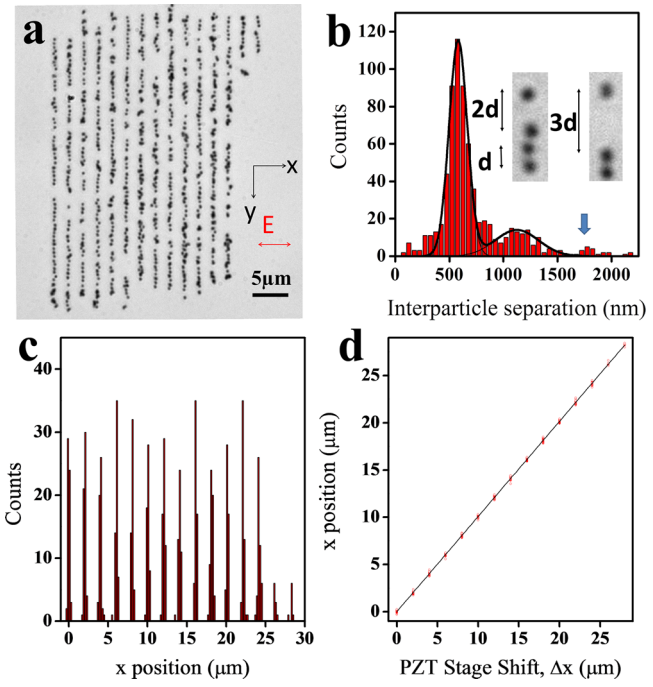

Figure 4. An optically printed nanoparticle array formed using a line trap. (a) A bright-field optical image of Ag nanoparticles deposited by an optical line trap to form a linear array. (b) The distribution of interparticle separations for Ag nanoparticles in the deposited arrays. The black curve is a two-peak Gaussian fit to the distribution with means and standard deviations of 580 ± 84 and 1125 ± 91 nm for the two peaks, respectively. The blue arrow indicates a small feature at 3× the separation that is expected from the optical binding interaction. Inset: optical images of representative examples that contribute to the peaks; d represents the separation of the primary peak in the distribution. The size of inset optical images is 1.0 × 3.3 μm. (c) Histogram of x-axis positions of deposited nanoparticle lines in (a). (d) x positions for silver nanoparticles as a function of PZT stage shift, Δx. The black line is a linear fit with the equation, $y = a + b*x$. a is the intercept of the fitting line, which is 0.0029 μm, and b is the slope of the fitting line, which is 1.007 ± 0.000. Note that the first column's position is 0.

a PEI-coated glass substrate (see videos S1 and S2 and the Supporting Information for details). Figure 4a shows a typical bright-field optical image of a Ag nanoparticle pattern (40 × 40 μm) with 2 μm steps along the x-direction (i.e., Δx = 2 μm column separation) on a PEI-modified glass substrate (coated at pH = 3.33). The optical image shows a nanoparticle array that is well-ordered on both micron- and nanoscales. It is also noteworthy that there is no spontaneous (random) deposition of Ag nanoparticles that occurred during the optical printing process. This means that the electrostatic repulsion was $>k_BT$ but not so large that the optical trapping forces could not overcome it.

The accuracy and precision of optical printing are assessed by determining the position variation of deposited nanoparticles vs the stage positions. Figure 4c shows the x-position distribution of deposited nanoparticle lines in Figure 4a; the x-position distribution of Ag nanoparticles in each line shows a narrow Gaussian peak (standard deviation ~ 110 nm), and the distance between adjacent peaks is about 2 μm. This position variation is quite small (i.e., the precision is good) considering the ~300 nm fwhm width of the line trap in the x-direction at a relatively low laser trap power density (30 mW/μm^2). Figure 4d shows the resulting plot of x positions of the nanoparticles vs the piezo stage shift (Δx) where the regression gives a measure of the accuracy (and absence of any significant distortion in the field of view) of the optical printing method. The agreement to a linear fit (slope = 1.007 ± 0.00 and an intercept of 0.0029 μm vs ideally zero) is a measure of the excellent accuracy along the x-direction reflecting the narrow (diffraction limited) transverse intensity profile of the optical trap.

The more interesting finding is the interparticle separation (center-to-center in the y-direction) of Ag nanoparticles in the array of Figure 4a. This distance distribution of adjacent Ag nanoparticles (from over 1000 nanoparticles) is shown in Figure 4b. The nanoparticles are well-separated with little aggregation in the Ag nanoparticle array shown in Figure 4a. The interparticle separation shows a dominant sharp peak centered at 580 nm (from a Gaussian fit), and the standard deviation of the main peak of the distribution is 84 nm. A second smaller peak occurs at ~1130 nm, which is at ~2 times the position of the main peak, and there is a hint of a third feature at ~1800 nm (see arrow in Figure 4b). The insets in Figure 4b show representative examples of deposited Ag nanoparticles in the extended lines showing defined gaps of 2d and 3d units of interparticle separation, where $d \approx$ 580 nm. The deposition rate of individual particles in the linear chain varies stochastically, and thus, some nanoparticles failed to be immobilized on the substrate while the stage was moved along y in 1 μm steps. However, a majority of Ag nanoparticles are separated with a distance associated with the primary peak (over 74% of the total deposited particles are in the range of the peak defined by the mean value $\pm 2\sigma$) even though we did not have a tightly defined optical trap along the y-direction. The excellent precision of particle deposition suggests the presence of a strong interparticle interaction and potential.

Electrodynamic Interparticle Interactions. The El-Sayed and Aussenegg groups reported the distance dependence of near-field interactions by creating structures by electron-beam lithography and measuring the spectral properties (e.g., red-shift of the spectra).[35,36] In contrast, we are studying interparticle interactions by establishing the influence of a previously deposited silver nanoparticle chain on the ordering of Ag nanoparticle deposition in subsequent chains as a function of the Δx shift of the optical line trap position. Figure 5a shows the measured intercolumn separation as a function of piezo (PZT) stage step size Δx. Three regimes with distinct deposition behaviors are observed: we term these non-interacting (green shaded), interacting (yellow), and unstable (pink/red) regimes. For a PZT step size of Δx > 600 nm, the deposition of particles in a subsequent chain is independent of the previous chain (i.e., noninteracting regime). For example, when the PZT step size is 1 μm, the average measured intercolumn separation is 1.01 μm (a typical image is shown as inset vi of Figure 5a). The standard deviation of the x-position of the deposited Ag nanoparticles is 107 nm, which is similar to that of nanoparticles with 2 μm separation (Figure 4b). The deposited nanoparticles were quite uniformly distributed, as can be seen from the dark-field scattering image (Figure S2, Supporting Information).

The interacting (yellow) regime is characterized by deviations from the expected intercolumn distance (PZT step size). In this regime, where Δx is in the range of 300−600 nm,

dx.doi.org/10.1021/jp506443t | J. Phys. Chem. C XXXX, XXX, XXX−XXX

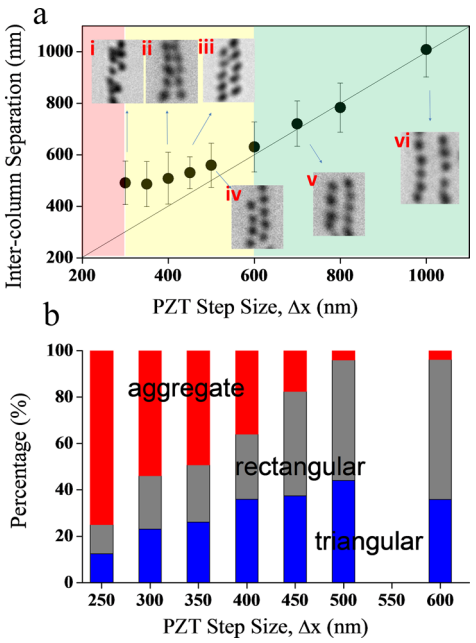

Figure 5. (a) Nanoparticle intercolumn separation vs piezo controlled step sizes (Δx). Inset: representative optical images of the deposited arrays for various step sizes: i, Δx = 0.3 μm; ii, 0.4 μm; iii, 0.45 μm; iv, 0.5 μm; v, 0.7 μm; vi, 1 μm. The size of optical images as insets are 3.1 × 2.5 μm. (b) The percentages of different arrangements (formations) of the deposited Ag nanoparticles as a function of PZT step size: red, near-field aggregation; gray, rectangular formation; and blue, triangular formation.

the x positions of the deposited Ag nanoparticles are dramatically different as compared to their target positions (i.e., the PZT step size). For example, when the PZT step size Δx = 450 nm, the x distance of depositing nanoparticles to the previously deposited column (intercolumn distance) is about 530 nm. A typical arrangement of nanoparticles is shown as inset iii of Figure 5a. Further decrease of the Δx step size exacerbates the mean deviation. The boundary of the interacting and unstable regimes for the experimental conditions used occurs between 250 and 300 nm. When the PZT step size is 300 nm, we are still able to deposit nanoparticles with defined spacing near the pre-existent chain, but the aggregation of Ag nanoparticles between the previous and newly deposited columns increases (inset i in Figure 5a). Further reducing the intercolumn distance (i.e., $\Delta x \leq 250$ nm) results in loss of control of the deposited particle positions; instead of immobilizing the Ag nanoparticles to a desired location, most deposited particles were stuck onto the existing chain, thus forming aggregates (they would be represented by points at intercolumn separation = 200 nm). This last behavior is the result of strong near-field interactions.

The deposited silver nanoparticles in the optical printing process can be classified into three types of configurations with respect to a pre-existing chain: rectangular formation, triangular formation, and aggregation. The percentages of configurations as a function of PZT step size are summarized in Figure 5b. It is evident that aggregation dominates when the PZT step size, Δx, is below 300 nm. Consistent with a previous study,[37] within this distance, the trapped nanoparticle has a high probability to be deposited in near-field contact. The rectangular and triangular ordering dominate in the yellow-shaded interacting regime. The rectangular and triangular ordering continues in the noninteracting regime, but we believe that this is related to our limited classification of configurations of random alignments since the long-range (>600 nm) interactions are weak.[25]

The characteristics of particle spacing and spatial configurations indicate that the metal nanoparticles interact on near-field scales and on the length scale of the trapping laser light being applied (800 nm/n, where n = 1.33 for water). The latter scale is that of optical binding of Ag nanoparticles in the optical trap, and here, we infer that the interaction also occurs with predeposited Ag nanoparticles on the substrate. We have shown that the optical binding interaction can result in coupled motions of nanoparticles in optical traps in solution, where they maintain a constant separation.[12,27,28,38] Silver nanoparticles arrays can be maintained as "rigid bodies" with a preferred separation of approximately 564 nm in aqueous solution showing that the interaction potential > k_BT.[25]

In the present experiment, the deposited nanoparticle array with well-defined row separations (along the y-direction, Figure 4b) demonstrates that the effect of optical binding is strongly preserved during the optical printing process. The primary peak (580 nm) for the interparticle separation in the chains is consistent with optical binding.[25] The existence of the two peaks in Figure 4b is also consistent with the expectations of the optical binding potential, which is periodic in the trapping laser wavelength. Furthermore, the observations in Figure 5 clearly demonstrate the existence of both attractive and repulsive interactions during optical printing when two Ag nanoparticle chains are separated at different distances. When the pre-existing nanoparticles are far from the newly defined position for deposition (Δx > 600 nm), the effect of the pre-existing silver chain is negligible. When we force deposition in close proximity to predeposited nanoparticles, aggregation (i.e., near-field interaction) dominates. In the 300−600 nm regimes, there is an electrodynamic repulsion. Overall, both intrachain optical binding forces (along the y-axis) and interchain interactions (along x) play critical roles in determining the locations of newly deposited Ag nanoparticles.

Moreover, the position difference between deposited nanoparticles and PZT step size as a function of PZT step size (Figure S3, Supporting Information) is well-fitted with a $1/\Delta x^3$ function, which indicates the existence of a repulsive force from optical binding interactions in the stable and yellow-shaded interacting regimes.[25,28] However, this functional dependence does not mean that only repulsive forces are important. A strong attractive interaction occurs in the near-field, but this is at smaller separations. In fact, it is this attraction that causes the formation of aggregates when the Δx separation is <250 nm.

SIMULATIONS AND DISCUSSION

We conducted simulations to corroborate these experimental observations and interpretation. Electrodynamic interactions can be modeled in finite-differential time-domain (FDTD) simulations calculating the electromagnetic (EM) field and forces for various particle arrangements. Figure 6 shows a model configuration; six spherical Ag nanoparticles (200 nm in diameter) were aligned in a linear chain along the y-axis with a separation of 585 nm. The intensity distribution of the electric field was calculated using a linearly polarized plane wave with λ = 800 nm (vacuum), which propagates in the z-direction and is polarized along the x-axis (Figure 6a). Interference from the coherent scattering of the laser beam and the deposited particles modifies the resultant total optical field; specifically, the intensity of the electromagnetic field around the midplane

dx.doi.org/10.1021/jp506443t | J. Phys. Chem. C XXXX, XXX, XXX−XXX

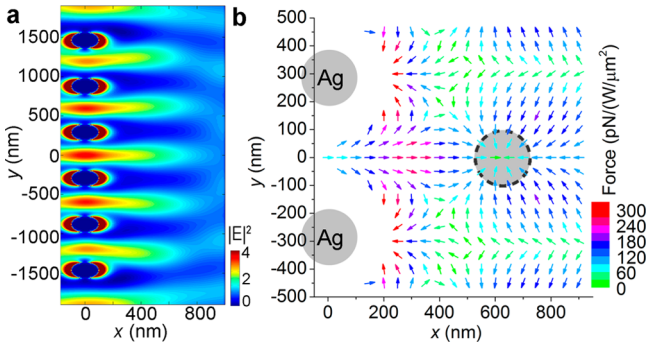

Figure 6. (a) FDTD simulation of optical-field distributions around linear chains of Ag nanoparticles. Image stretch factor (X/Y) is 1.8. (b) Map of the force exerted by the central pair of 200 nm diameter Ag nanoparticles (the gray spheres) on a new 200 nm Ag nanoparticle in water illuminated by a plane wave (800 nm vacuum wavelength). The polarization is along the x-axis. The direction of each arrow denotes the direction of the optical force when the third nanoparticle is located at the midpoint of the arrow. The colors of the arrows represent the value of electrodynamic forces as shown by the scale bar. The direction indicates the (local) direction of the force with respect to the pair of fixed particles. The dashed circle represents the equilibrium position of the newly added nanoparticle.

between adjacent Ag nanoparticles in the chain is increased. Since the width of the optical line trap is ~300 nm, when the separation between two deposited Ag nanoparticle chains is <600 nm, the previously deposited Ag nanoparticle chain will modify the line trap and strongly influence the deposition of the new Ag nanoparticle chain.

Figure 6b shows the optical forces exerted by the central pair of deposited Ag nanoparticles in the chain on a new nanoparticle at various x, y locations. The force map shows that there is an equilibrium position at (620, 0) nm where the optical force becomes zero. This equilibrium position becomes closer to the chain when there are fewer deposited nanoparticles, but the triangular configuration is maintained (Supporting Information, Figure S4), as suggested in Figure 6a and observed in the experimental results of Figure 5. For interparticle separations smaller than the equilibrium position, the deposited nanoparticles exert repulsive forces on the new (probe) nanoparticle that become stronger when the distance from the deposited nanoparticles decreases (Supporting Information, Figure S4c). This repulsive interaction at smaller separation implies that the next chain of deposited nanoparticles should tend to have a positive deviation if the transverse (x-direction) shift of the optical line trap is less than the equilibrium separation along the x-axis. Overall, the simulation results support our experimental findings and their explanation in terms of optical binding interactions.

CONCLUSION

We have demonstrated electrodynamic assembly and deposition of silver nanoparticle chains and arrays onto solid substrates using a simple and facile optical printing approach. We show that the electrostatic charge of the substrate surface, obtained by depositing PEI at various pH values, allows optimizing this parameter to prevent spontaneous particle deposition. The electrodynamic interaction termed optical binding plays a critical role in determining the interparticle separations in assembled nanoparticle chains and arrays. Furthermore, the electrodynamic interaction of pre-existing Ag nanoparticle chains on the deposition of subsequent silver nanoparticles is studied, revealing strong repulsion when the optically trapped nanoparticles are brought closer than the optimal optical binding separation. Optical printing as demonstrated here combines aspects of guided assembly and directed self-organization, yet with high (<100 nm) precision. We are employing optically printed metal nanoparticle arrays for quantum optics experiments and in studies of the enhancement in sensing afforded by mesoscale (as opposed to near-field) field enhancements.

ASSOCIATED CONTENT

Supporting Information

Detailed methodology, additional figures, and discussion are found in the Supporting Information. This material is available free of charge via the Internet at http://pubs.acs.org.

AUTHOR INFORMATION

Corresponding Author

*E-mail: nfschere@uchicago.edu (N.F.S.).

Notes

The authors declare no competing financial interest.

ACKNOWLEDGMENTS

This work was supported by a grant from the National Science Foundation (CHE-1059057) and partial support from the National Security Science and Engineering Faculty Fellowship (NSSEFF) program. We thank the University of Chicago NSF-MRSEC (DMR-0820054) for central facilities support. We thank Raman Shah for helpful discussions.

REFERENCES

(1) Li, J.; Cushing, S. K.; Zheng, P.; Meng, F.; Chu, D.; Wu, N. Plasmon-Induced Photonic and Energy-Transfer Enhancement of Solar Water Splitting by a Hematite Nanorod Array. *Nat. Commun.* **2013**, *4*, 2651.

(2) Gong, X.; Bao, Y.; Qiu, C.; Jiang, C. Individual Nanostructured Materials: Fabrication and Surface-Enhanced Raman Scattering. *Chem. Commun.* **2012**, *48*, 7003−7018.

(3) Sharma, B.; Frontiera, R. R.; Henry, A.-I.; Ringe, E.; Van Duyne, R. P. SERS: Materials, Applications, and the Future. *Mater. Today* **2012**, *15*, 16−25.

(4) Henzie, J.; Andrews, S. C.; Ling, X. Y.; Li, Z. Y.; Yang, P. D. Oriented Assembly of Polyhedral Plasmonic Nanoparticle Clusters. *Proc. Natl. Acad. Sci. U.S.A.* **2013**, *110*, 6640−6645.

(5) Jeong, H. E.; Kim, I.; Karam, P.; Choi, H. J.; Yang, P. D. Bacterial Recognition of Silicon Nanowire Arrays. *Nano Lett.* **2013**, *13*, 2864−2869.

(6) Leggett, G. J. Direct Writing of Metal Nanostructures: Lithographic Tools for Nanoplasmonics Research. *ACS Nano* **2011**, *5*, 1575−1579.

(7) Marago, O. M.; Jones, P. H.; Gucciardi, P. G.; Volpe, G.; Ferrari, A. C. Optical Trapping and Manipulation of Nanostructures. *Nat. Nano* **2013**, *8*, 807−819.

(8) Solis, D.; Willingham, B.; Nauert, S. L.; Slaughter, L. S.; Olson, J.; Swanglap, P.; Paul, A.; Chang, W.-S.; Link, S. Electromagnetic Energy Transport in Nanoparticle Chains via Dark Plasmon Modes. *Nano Lett.* **2012**, *12*, 1349−1353.

(9) Jeevan, M. M.; William, M. C.; May, P. S.; QuocAnh, L.; Grant, A. C.; Jon, J. K. Security Printing of Covert Quick Response Codes Using Upconverting Nanoparticle Inks. *Nanotechnology* **2012**, *23*, 395201.

(10) Swanglap, P.; Slaughter, L. S.; Chang, W. S.; Willingham, B.; Khanal, B. P.; Zubarev, E. R.; Link, S. Seeing Double: Coupling between Substrate Image Charges and Collective Plasmon Modes in

Self-Assembled Nanoparticle Superstructures. *ACS Nano* **2011**, *5*, 4892−4901.
(11) Radha, B.; Kulkarni, G. U. An Electrical Rectifier Based on Au Nanoparticle Array Fabricated Using Direct-Write Electron Beam Lithography. *Adv. Funct. Mater.* **2012**, *22*, 2837−2845.
(12) Demergis, V.; Florin, E. L. Ultrastrong Optical Binding of Metallic Nanoparticles. *Nano Lett.* **2012**, *12*, 5756−5760.
(13) Iida, T. Control of Plasmonic Superradiance in Metallic Nanoparticle Assembly by Light-Induced Force and Fluctuations. *J. Phys. Chem. Lett.* **2012**, *3*, 332−336.
(14) Yan, Z. J.; Jureller, J. E.; Sweet, J.; Guffey, M. J.; Pelton, M.; Scherer, N. F. Three-Dimensional Optical Trapping and Manipulation of Single Silver Nanowires. *Nano Lett.* **2012**, *12*, 5155−5161.
(15) Pelton, M.; Liu, M. Z.; Kim, H. Y.; Smith, G.; Guyot-Sionnest, P.; Scherer, N. E. Optical Trapping and Alignment of Single Gold Nanorods by Using Plasmon Resonances. *Opt. Lett.* **2006**, *31*, 2075−2077.
(16) Tong, L.; Righini, M.; Gonzalez, M. U.; Quidant, R.; Kall, M. Optical Aggregation of Metal Nanoparticles in a Microfluidic Channel for Surface-Enhanced Raman Scattering Analysis. *Lab Chip* **2009**, *9*, 193−195.
(17) Toussaint, K. C.; Liu, M.; Pelton, M.; Pesic, J.; Guffey, M. J.; Guyot-Sionnest, P.; Scherer, N. F. Plasmon Resonance-Based Optical Trapping of Single and Multiple Au Nanoparticles. *Opt. Express* **2007**, *15*, 12017−12029.
(18) Hansen, P. M.; Bhatia, V. K.; Harrit, N.; Oddershede, L. Expanding the Optical Trapping Range of Gold Nanoparticles. *Nano Lett.* **2005**, *5*, 1937−1942.
(19) Pauzauskie, P. J.; Radenovic, A.; Trepagnier, E.; Shroff, H.; Yang, P.; Liphardt, J. Optical Trapping and Integration of Semiconductor Nanowire Assemblies in Water. *Nat. Mater.* **2006**, *5*, 97−101.
(20) Urban, A. S.; Lutich, A. A.; Stefani, F. D.; Feldmann, J. Laser Printing Single Gold Nanoparticles. *Nano Lett.* **2010**, *10*, 4794−4798.
(21) Ito, S.; Yoshikawa, H.; Masuhara, H. Laser Manipulation and Fixation of Single Gold Nanoparticles in Solution at Room Temperature. *Appl. Phys. Lett.* **2002**, *80*, 482−484.
(22) Guffey, M. J.; Scherer, N. F. All-Optical Patterning of Au Nanoparticles on Surfaces Using Optical Traps. *Nano Lett.* **2010**, *10*, 4302−4308.
(23) Nedev, S.; Urban, A. S.; Lutich, A. A.; Feldmann, J. Optical Force Stamping Lithography. *Nano Lett.* **2011**, *11*, 5066−5070.
(24) Do, J.; Fedoruk, M.; Jäckel, F.; Feldmann, J. Two-Color Laser Printing of Individual Gold Nanorods. *Nano Lett.* **2013**, *13*, 4164−4168.
(25) Yan, Z.; Shah, R. A.; Chado, G.; Gray, S. K.; Pelton, M.; Scherer, N. F. Guiding Spatial Arrangements of Silver Nanoparticles by Optical Binding Interactions in Shaped Light Fields. *ACS Nano* **2013**, *7*, 1790−1802.
(26) Yan, Z.; Gray, S. K.; Scherer, N. F. Potential Energy Surfaces and Reaction Pathways for Light-Mediated Self-Organization of Metal Nanoparticle Clusters. *Nat. Commun.* **2014**, *5*, 3751.
(27) Burns, M. M.; Fournier, J. M.; Golovchenko, J. A. Optical Binding. *Phys. Rev. Lett.* **1989**, *63*, 1233−1236.
(28) Dholakia, K.; Zemanek, P. Colloquium: Gripped by Light: Optical Binding. *Rev. Mod. Phys.* **2010**, *82*, 1767−1791.
(29) Yan, Z.; Manna, U.; Qin, W.; Camire, A.; Guyot-Sionnest, P.; Scherer, N. F. Hierarchical Photonic Synthesis of Hybrid Nanoparticle Assemblies. *J. Phys. Chem. Lett.* **2013**, *4*, 2630−2636.
(30) Guffey, M. J.; Miller, R. L.; Gray, S. K.; Scherer, N. F. Plasmon-Driven Selective Deposition of Au Bipyramidal Nanoparticles. *Nano Lett.* **2011**, *11*, 4058−4066.
(31) Israelachvili, J. N. *Intermolecular and Surface Forces*, 3rd ed.; Academic Press: Burlington, MA, 2011; pp 1−674.
(32) Demadis, K. D.; Paspalaki, M.; Theodorou, J. Controlled Release of Bis(Phosphonate) Pharmaceuticals from Cationic Biodegradable Polymeric Matrices. *Ind. Eng. Chem. Res.* **2011**, *50*, 5873−5876.
(33) Ziebarth, J. D.; Wang, Y. Understanding the Protonation Behavior of Linear Polyethylenimine in Solutions through Monte Carlo Simulations. *Biomacromolecules* **2009**, *11*, 29−38.
(34) Decher, G. Fuzzy Nanoassemblies: Toward Layered Polymeric Multicomposites. *Science* **1997**, *277*, 1232−1237.
(35) Rechberger, W.; Hohenau, A.; Leitner, A.; Krenn, J. R.; Lamprecht, B.; Aussenegg, F. R. Optical Properties of Two Interacting Gold Nanoparticles. *Opt. Commun.* **2003**, *220*, 137−141.
(36) Tabor, C.; Murali, R.; Mahmoud, M.; El-Sayed, M. A. On the Use of Plasmonic Nanoparticle Pairs as a Plasmon Ruler: The Dependence of the Near-Field Dipole Plasmon Coupling on Nanoparticle Size and Shape. *J. Phys. Chem. A* **2008**, *113*, 1946−1953.
(37) Svedberg, F.; Li, Z.; Xu, H.; Käll, M. Creating Hot Nanoparticle Pairs for Surface-Enhanced Raman Spectroscopy through Optical Manipulation. *Nano Lett.* **2006**, *6*, 2639−2641.
(38) Burns, M. M.; Fournier, J. M.; Golovchenko, J. A. Optical Matter - Crystallization and Binding in Intense Optical-Fields. *Science* **1990**, *249*, 749−754.